Shape transitions and island nucleation for Si/Ge molecular beam epitaxy on stripe-patterned Si (001) substrate

B. Sanduijav,[1,*] D. Matei,[1,2] G. Chen,[1] and G. Springholz[1,†]
[1]*Institut für Halbleiter- und Festkörperphysik, Johannes Kepler University, A-4040 Linz, Austria*
[2]*National Institute for Laser, Plasma and Radiation Physics, RO-077125 Bucharest, Romania*
(Received 18 July 2009; revised manuscript received 20 August 2009; published 24 September 2009)

Si and Ge growth on the stripe patterned Si (001) substrates is studied using scanning tunneling microscopy. During Si buffer growth, the stripe morphology rapidly evolves from multifaceted "U" to "V"-shaped forms. This involves successive transitions between different low energy {11*n*} side facets, where *n* continuously decreases from $n=3$ to 20. Ge growth on such stripes induces the formation of a pronounced side wall ripple structure when the Ge thickness exceeds three monolayers. This ripple structure consists of alternating {105} microfacets oriented perpendicularly to the stripes. Depending of the side wall geometry, Ge nanoislands subsequently nucleate either on the side walls or at the bottom of grooves. The latter only occurs for "V"-shaped stripes, where the side wall ripples extend all the way from the top to the bottom of the grooves, allowing efficient downward mass transport. For multifaceted "U" stripes, the side wall ripples are interrupted by steeper side wall segments such that mounds and subsequently, pyramids and domes grow on the side walls instead of at the bottom of the grooves. The island shapes strongly depend on their position on the pattern topography, which also affects the critical coverage for island nucleation as well as for the transition from pyramids to domes. The mechanisms for nucleation at different positions are clarified by detailed analysis and the role of kinetic as well as energetic factors identified.

DOI: 10.1103/PhysRevB.80.125329 PACS number(s): 81.07.Ta, 81.15.Hi, 81.16.Dn, 68.37.Ef

I. INTRODUCTION

Self-organized Stranski-Krastanow island growth on prepatterned substrates has attracted tremendous interest[1–19] because it provides an effective pathway for controlled positioning of quantum dots in nanoelectronic devices and allows the fabrication of perfectly ordered quantum dot arrays that can even be stacked in three dimensions.[4,7–9] Site-controlled growth on predefined substrate locations requires a tight control over the pattern morphology and growth conditions.[6–18] In addition, sufficiently thick buffer layers have to be deposited in order to remove the defects induced by the patterning process to yield quantum dots with excellent structural and electronic properties.[6–13] During buffer growth, however, the pattern morphology rapidly changes. As a result, a complex surface topography is formed[9–15] that strongly affects the island nucleation process. In fact, depending on the pattern morphology, self-assembled quantum dots have been found to nucleate at different locations of the pattern structure such as at the bottom of pits, at the side walls or even at the top of ridges or mesa patterns (see Refs. 9–14). Therefore, a detailed understanding of the surface evolution during buffer layer growth as well as its effect on island nucleation is required for control of the self-organization process.

In the present work, *in situ* scanning tunneling microscopy is employed to unravel the complex morphology evolution of Si/Ge growth on stripe patterned Si (001) substrate templates. Because of their simple geometry, one-dimensional stripes represent a model system for the growth on nonplanar surfaces with complex pattern geometries. In the first part of the work, we show that already during Si buffer layer growth, a rapid characteristic transformation from multifaceted "U"- to "V"-shaped grooves occurs due to successive transitions from steep {113} to shallower {114}, {115}, and {119} side wall facets as growth proceeds. The speed of this transition strongly depends on the growth conditions and filling factor of the stripes. Therefore, both parameters have to be adjusted in order to obtain a well-defined stripe geometry. In the second part of the paper, Ge growth on stripes with different geometries is studied. It is shown that at a critical coverage of three monolayers, a pronounced side wall ripple structure appears perpendicular to the stripes due to microfaceting of the Ge surface. For "V"-shaped stripes, these ripples extend from the top to the bottom of the grooves, where subsequently, Ge islands are formed due to efficient downward mass transport. On the contrary, for multifaceted "U" stripes, the side wall ripples are interrupted by steeper side wall segments such that mounds, pyramids and domes form along the side walls of the stripes. Moreover, the island shapes depend on their position on the pattern topography and range from square pyramids, to asymmetric pyramids or even elongated {105} prisms for steeper grooves, but all eventually transform into domes at higher Ge coverages. The groove geometry also affects the critical coverages for island nucleation as well as the critical island sizes for shape transitions. By analysis of the details of the surface evolution, the mechanism for island growth at different positions is clarified, demonstrating that kinetic as well as energetic factors are important in this self-organization process.

II. EXPERIMENTAL

The investigations were carried out in a multichamber Si/Ge molecular beam epitaxy and scanning tunneling microscopy (STM) system[20] equipped with a solid source Si e-beam evaporator, a Ge effusion cell and Omicron VT-STM. Stripe patterned Si (001) substrates were prepared by electron beam or holographic lithography and CF_4 reactive ion

 ©2009 The American Physical Society

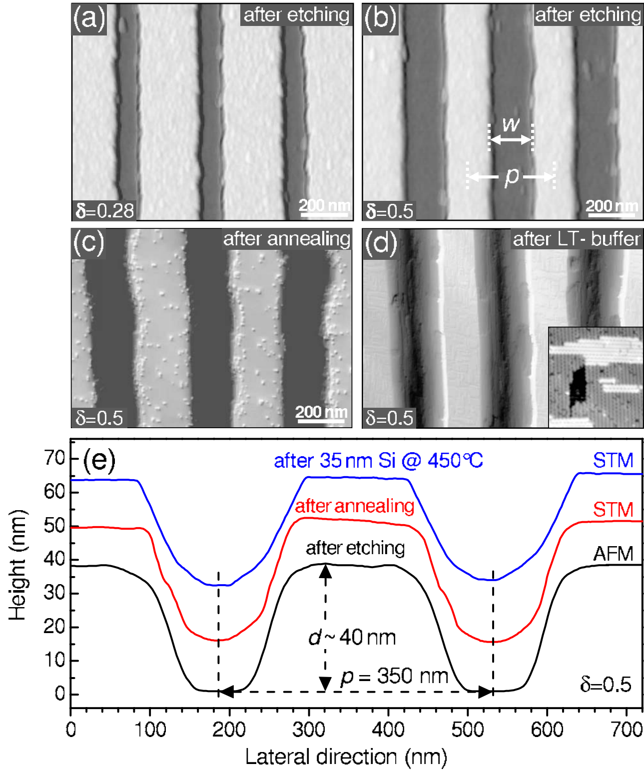

FIG. 1. (Color online) Top row: AFM images of stripe-patterned Si substrates after reactive ion etching showing stripes with two different filling factors $\delta = w/p = 0.28$ and 0.5 for (a) and (b), respectively, but constant period $p = 350$ nm. Middle row: STM images of stripes after annealing at 750 °C (c) and after subsequent 35 nm low temperature Si buffer growth at 450 °C (d). The insert in (d) shows the (2×1) reconstructed Si surface on the ridges on a magnified scale. Bottom: comparison of the cross-sectional stripe profiles after etching (bottom), after 5 min annealing at 750 °C (middle) and after 35 nm low temperature Si buffer growth (top).

etching. All stripes were aligned along the in-plane [110] direction and have a lateral period p of 350 nm. The grooves between the stripes were etched down to a depth d of 35 nm. By varying the exposure dose, different groove widths w ranging from 70 to 280 nm were obtained, which is characterized by a filling factor δ defined as ratio of the groove width to the lateral period, i.e., $\delta = w/p$. After patterning, the samples were characterized by atomic force microscopy (AFM) as is exemplified by Figs. 1(a) and 1(b) for patterns with filling factor $\delta = 0.28$ and 0.5, respectively. After reactive ion etching, the samples were cleaned with oxygen plasma, Piranha etch, and the RCA procedure.[21] Since the usual oxide desorption at temperatures above 900 °C leads to very rapid changes in the pattern morphology,[22] the native silicon dioxide was removed by a 5% HF dip. The resulting hydrogen passivated samples were immediately loaded into the multichamber vacuum system where, after outgassing at 350 °C, the samples were annealed at 600 °C for 30 min and finally at 750 °C for hydrogen desorption. Subsequent epitaxial growth was performed at substrate temperatures between 450 to 600 °C and growth rates of around 3 and 1 Å/min for Si and Ge, respectively, which were determined by a quartz thickness monitor as well as by *in situ* reflection high-energy electron diffraction (RHEED) intensity oscillations. The background pressure during growth was below 1×10^{-9} mbar and the substrate temperature was measured with an optical pyrometer. For imaging of the epitaxial surface structure, the samples were rapidly quenched to room temperature after different stages of growth and then transferred under UHV to the attached STM chamber. STM images were recorded with tunneling currents around 0.1 nA and a sample bias of 2–4 V. With a base pressure in the 10^{-11} mbar regime, sample growth could be continued afterwards, in which case the samples were shortly annealed for a few minutes at moderate temperatures around 500 °C.

III. SURFACE EVOLUTION DURING SI BUFFER LAYER GROWTH

Reactive ion etching of the substrates results in surfaces with a substantial amount of processing defects and surface roughness as is illustrated by the AFM images depicted in Figs. 1(a) and 1(b). After RCA cleaning, HF dipping, and UHV high-temperature annealing at 750 °C, carbon-induced clusters[23,24] remain on the surface as is demonstrated by the STM image of Fig. 1(c) recorded directly after the annealing step. These surface clusters could not be eliminated by repeated chemical cleaning of the Si wafers, and annealing at higher temperatures was found to result in a degradation of the pattern structure. Thus, Si buffer layer growth is essential prior to Ge deposition. This buffer growth has to be carried out at rather low temperatures because growth above 550 °C leads to a complete pattern erasure within few nm Si deposition. In the present work, a two-step buffer growth procedure was employed. The first step consisted of 35 nm Si deposited at a temperature of 450 °C. As proven by the STM image of Fig. 1(d), this effectively buries the carbon impurities on the surface and the Si surface on the ridges becomes atomically flat, exhibiting only monolayer steps and the usual (2×1) Si surface reconstruction (see insert). In spite of the low growth temperature, already some rounding of the bottom of the grooves occurs but the initial depth of the grooves is essentially preserved. This is indicated by the comparison of the cross-sectional profiles across the stripes before and after buffer layer growth depicted in Fig. 1(e).

To improve the surface quality and smoothen the still rather rough sidewalls of the grooves, the low temperature buffer growth step was followed by a second Si buffer growth at a higher temperature of 520 °C. During the second Si buffer growth, the surface morphology rapidly evolves due to enhanced surface diffusion. This is illustrated by the sequence of STM images displayed in Fig. 2 obtained after different stages of growth. Already after 7 nm Si at 520 °C, the grooves assume a well-defined multifaceted "U" shape, as is demonstrated by the STM image of Fig. 2(a) for stripes with filling factor $\delta = 0.5$. As shown by the cross-sectional profile depicted on the right hand side of Fig. 2(a), the side walls are composed of two short segments with ~9° inclination at the top and bottom of the grooves, and a steeper middle segment with ~25° inclination. The orientation of the side wall faces can be directly deduced from the surface orientation map (SOM) of the STM image, in which the

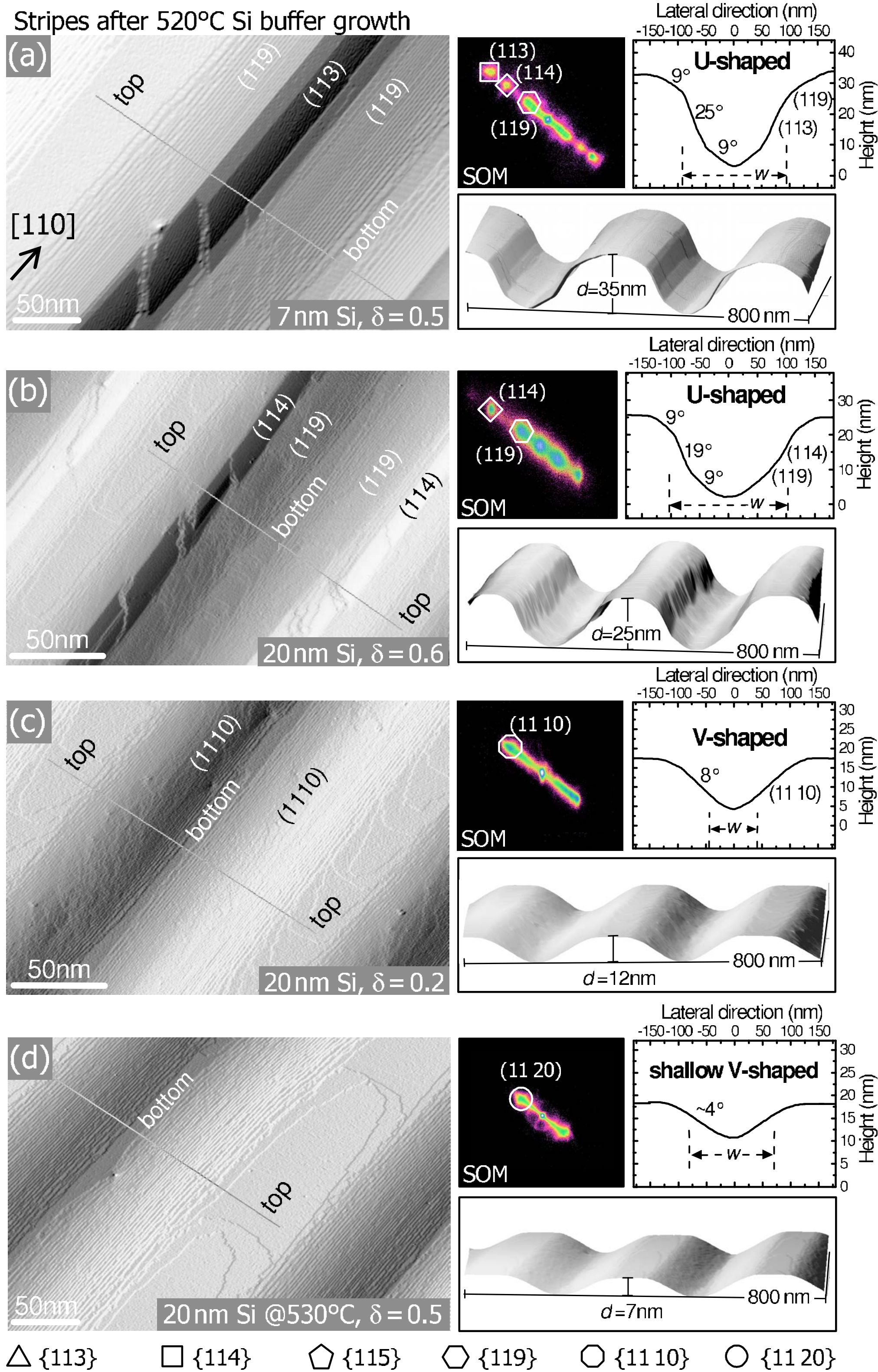

FIG. 2. (Color online) Evolution of the stripe morphology during second 520 °C Si buffer growth as revealed by STM images (left-hand side), surface orientation maps (SOM, center) and surface profiles (right hand side). (a) "U"-shaped stripes with {113} facets formed after 7 nm Si deposition, (b) shallower "U" stripes with flatter {114} facets after 20 nm Si deposition, (c) "V"-shaped stripes with shallow {11 10} facets formed after 20 nm Si on stripes with smaller filling factor $\delta=0.2$, (d) shallow "V" grooves with {11 20} facets formed after 2 nm Si growth at a higher temperature of 530 °C. The side wall angles of the grooves and the original stripe widths w are indicated on the cross-sectional profiles on the right hand side. The facet spots in the SOMs are labeled by the symbols as depicted below. The change in stripe geometry is visualized by the 3D STM images depicted on the right hand side on equal scale.

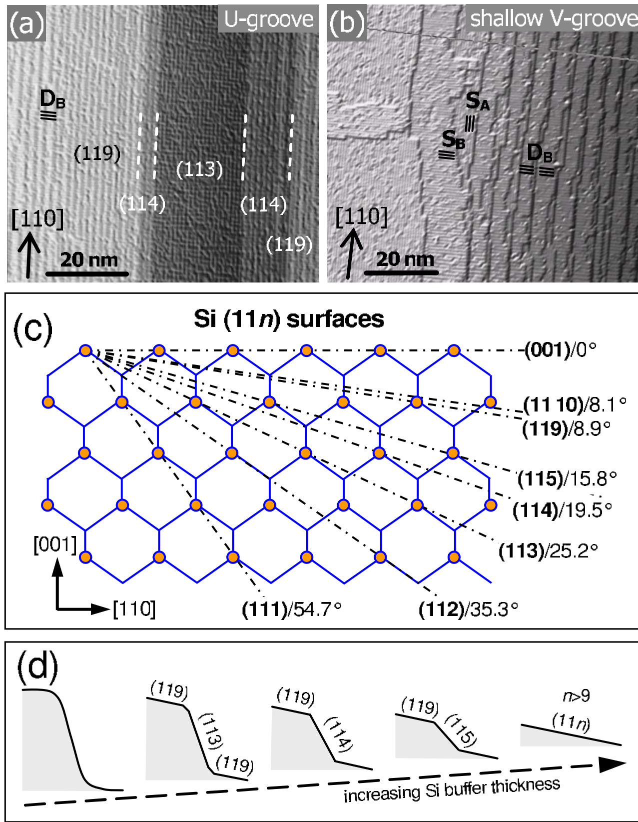

FIG. 3. (Color online) Top: high-resolution STM images of the side wall structure of the stripes with (a) multifaceted "U" geometry [cf. Fig. 2(a)] and (b) with a shallow {11 20} "V" geometry with 4° side wall inclination [cf. Fig. 2(d)]. Middle: (c) side view of the silicon crystal lattice perpendicular to the stripe direction. The dash-dotted lines indicate the high-indexed (11*n*) facet surfaces observed on the side wall of the stripes. Bottom: (d) schematic illustration of the successive shape transformation of the stripes occurring with increasing Si buffer thickness.

intensity of each spot represents the relative amount of surface area within the STM image with orientation defined by the position (distance and azimuth angle) of the spot relative to the central (001) spot. The resulting surface orientation map is shown in the middle panel of Fig. 2(a) and exhibits four distinct satellite spots corresponding to {113} and {114} facets and two broader inner maxima around the {119} surface orientation as marked by the different symbols of △, □, and ⬡, respectively. The corresponding inclination angles of 25°, 19°, and 9° agree well with those obtained from the surface profiles. Therefore, the side wall faces are composed of {113} and {114} middle facets, which pass over to shallower {119} segments toward the top and the bottom of the grooves.

The step structure of the side wall facets is clearly resolved by the high-resolution STM image depicted in Fig. 3(a). It reveals that the {119} areas are actually composed of regularly spaced D_B type double monolayer steps with an average spacing of 17 Å. In agreement with the work of Baski *et al.*,[25] the {119} surface areas are therefore composed of three dimer rows alternating with a rebonded double step [see schematic illustration of Fig. 3(c)], where the rebonded double step lowers the free energy of the surface.[26] Whereas the {119} areas have the character of a vicinal surface, the steeper side wall facets appear completely flat and step-free in the STM image and display the same atomic arrangement observed on singular (113) and (114) Si surfaces.[25,27,28] The (114) surface unit cell thus, consists of one dimer and a rebonded double monolayer step.[25] The (113) surface exhibits a (3×2) reconstruction composed of alternating dimers and tetramers, as has been discussed in detail in Refs. 29–31. The vicinal character of the {119} side wall faces compared to the singular {113} and {114} faces is corroborated by the strong elongation and broadening of the {119} spots in the surface orientation map of Fig. 2(a) whereas the spots arising from the {113} and {114} facets are sharp and well-defined.

Continuing Si buffer growth leads to a rapid shrinking of the middle side wall segment and a concomitant expansion of the shallower upper and lower {119} segments. This is demonstrated by the STM image of Fig. 2(b) recorded after 20 nm Si deposition. The line profile depicted on the right hand side identifies inclinations of ~9° at the upper and lower edge of the grooves and of ~19° for the middle segment. Thus, the {113} facet has been completely replaced by a {114} facet and accordingly, only the {114} and {119} spots appear in the surface orientation map. In addition, the groove depth is reduced to 25 nm, as shown by the line profile in Fig. 2(b). With further increasing buffer thickness, the {114} segment also shrinks and is replaced by a short {115} segment, which also disappears during further deposition such that only one extended ~9° side wall surface remains. The surface profile then assumes a "V"-like shape as demonstrated by the STM image of Fig. 2(c). The characteristic sequence of surface transformations from steeper to shallower {11*n*} sidewall facets is illustrated schematically in Fig. 3(d) and results in a continuous decrease in the groove depth as the buffer thickness increases.

The speed of the transformation process strongly depends on the initial width and depth of the grooves and is found to be much faster for narrow grooves with small filling factors δ. This is exemplified by Fig. 2(c) for a pattern with $\delta=0.2$ where already after 20 nm Si deposition the stripes are completely transformed from "U" to "V" shaped and the depth reduced to only 12 nm. Correspondingly, the surface orientation map of Fig. 2(c) exhibits only two elongated maxima around the {11 10} orientation and all other facet spots have completely disappeared. The corresponding cross-sectional profile depicted in Fig. 2(c) exhibits a maximum inclination angle of 8° in the sidewall middle, which continuously decreases toward the top and bottom of the grooves. Therefore, the sidewall is no longer composed of a well-defined stable facet, in agreement with STM studies of vicinal Si surfaces.[25,32] This conclusion is also supported by observation of a large elongation of the {11 10} SOM maxima, which span over surface inclinations ranging from 3° to 8°.

Further Si deposition leads to the formation of even shallower "V" grooves and a completely planar surface is rapidly reformed. The STM image of such a transient shallow "V" groove with only 4° sidewall inclination is shown in Fig. 2(d), where the buffer growth was carried out at a slightly higher temperature of 530 °C, which speeds up the planarization process. As shown by Fig. 2(d), the surface orien-

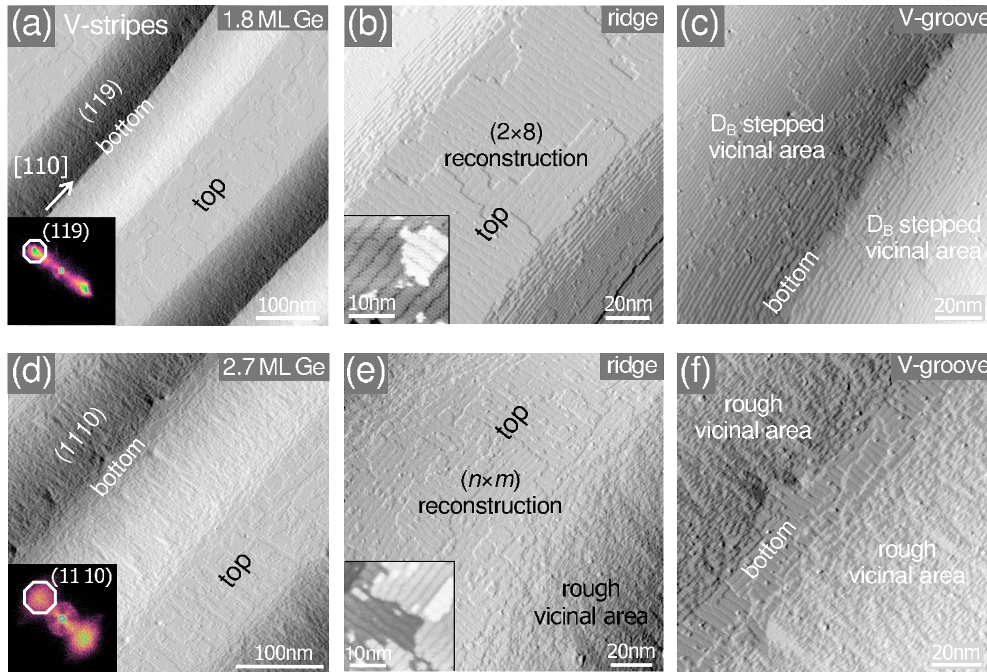

FIG. 4. (Color online) STM images of "V"-shaped stripes during initial Ge deposition recorded after 1.8 ML Ge at 520 °C [top row (a)–(c)] and additional 0.9 ML Ge to 2.7 ML at 600 °C [bottom row (d)–(f)]. The initial stripe geometry contained mainly {119} side wall faces as shown in Fig. 2(c). The facet spots are indicated in the surface orientation maps shown as insets. Details of the surface reconstruction and step structures on the ridges as well as the side walls of the grooves are shown by the higher-resolution STM images depicted on the right hand side.

tation map in this case only shows two elongated maxima at around {11 20} and the groove depth is reduced to 7 nm. Like for the {11 10} surfaces, the sidewalls are again formed by a regular step train perpendicular to the stripes, indicating a vicinal side wall surface. The higher-resolution STM image displayed in Fig. 3(b) shows that the D_B-stepped terrace structure is formed by merging of S_A and S_B single steps in the transitional region at the top of the grooves, where the width of the (2×1) reconstructed (001) terraces increases continuously toward the ridge of the stripes. This agrees with previous STM studies on vicinal Si (001) surfaces where for miscut angles less than 2° a stepped (2×1) surface with single monolayer steps was found[33,34] that evolves toward a double monolayer stepped surface at higher miscut angles.[35] Obviously, the shallow "V"-groove structure is highly unstable during Si deposition because downward diffusion of Si adatoms and incorporation at step edges leads to a very rapid filling and planarization of the grooves. Thus, it is essential to keep the second Si buffer thickness at 20 nm or below in order to preserve the structure of the patterned substrate templates.

IV. GE GROWTH ON "V"-SHAPED STRIPES

To study the influence of the stripe geometry on subsequent Ge growth, we first focus on stripes with "V" geometry obtained by 20–25 nm 520 °C Si buffer growth. These "V" stripes exhibit predominant {119} side wall facets with 9° inclination and a depth of about 15 nm. In the first growth step, 1.8 ML Ge was deposited at 520 °C directly after Si buffer growth without growth interruption. As evidenced by the STM image depicted in Fig. 4(a), this does not change the "V" geometry of the stripes, i.e., the {119} side walls and flat surface ridges are completely preserved. This is also proven by the corresponding surface orientation map depicted as insert, which only shows two spots at the {119} positions. Thus, up to this coverage a conformal two-dimensional (2D) Ge wetting layer growth occurs. The zoomed-in STM image of the top of the ridges displayed in Fig. 4(b) reveals that a strain-induced (2×8) surface reconstruction is formed on the (001) Ge wetting layer surface.[36–39] It consists of a periodic array of dimer vacancy lines, which appear as dark depressions in the STM images and allow a partial strain relaxation of the wetting layer.[38–42] The spacing of the dimer vacancy lines is ~3 nm, which according to Voigtländer *et al.*[38,39] indicates a ~20% Si/Ge intermixing within the wetting layer. On the side walls of the grooves [see Fig. 4(c)], a regular double D_B step structure with average 2 nm spacing is formed and the sharp intersection of the "V"-groove bottom is preserved at this growth temperature.

Increasing the Ge coverage by 0.9 ML at 600 °C to a total thickness of 2.7 ML significantly changes the surface structure. This is demonstrated by the STM images displayed in the lower panel of Fig. 4. Although the overall stripe morphology is still preserved [see large-scale STM image of Fig. 4(d)], a significant roughening occurs on the side walls as well as the ridges of the stripes. This is revealed by the higher-resolution STM images displayed in Figs. 4(e) and 4(f) and is also evidenced by the significant broadening of the facet spots in the surface orientation map shown in Fig.

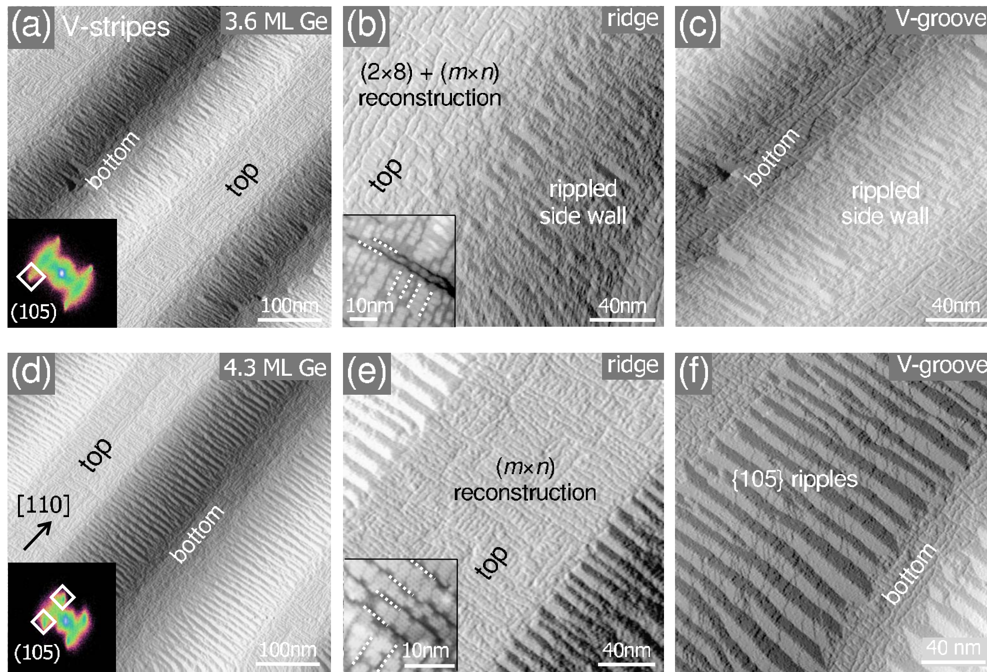

FIG. 5. (Color online) STM images of "V"-shaped stripes after 3.6 ML Ge [top (a) to (c)] and 4.3 ML Ge deposition [bottom (d)–(e)] at 600 °C, showing the onset of {105} side wall ripple formation. This is also evidenced by the corresponding surface orientation maps shown as inserts. The zoomed-in STM images of the grooves and ridges are depicted on the right hand side, where the latter reveal the formation of dimer vacancy lines on the Ge wetting layer surface, as indicated by the dotted lines in the high-resolution STM inserts of (b) and (e).

4(d) as insert. In addition, a slight decrease in the side wall inclination to 8° occurs such that the surface orientation map peaks are shifted to the {11 10} position. On the (001) ridges, apart from the dimer vacancy lines, additional monolayer islands are formed on the wetting layer surface [see Fig. 4(e)]. This is attributed to an increased ad-atom density on the terraces due to the reduced sticking probability at surface steps induced by increasing strain,[39] which enhances 2D islands nucleation and roughening of the terraces. At the same time, the parallel and nearly straight D_B double steps on the side walls of the grooves break up such that a rather rough vicinal surface is formed with a substantial corrugation of the step edges. This is shown in detail by the STM image of Fig. 4(f) and is similar to what has been observed for Ge growth on vicinal Si surfaces.[43] At this growth temperature of 600 °C also a slight flattening of the bottom of the "V" grooves occurs.

Further increasing the Ge coverage to 3.6 ML leads to a pronounced surface roughening on the ridges as well as the side walls of the grooves as shown by the STM images displayed in Fig. 5. On the ridges, the 2D island density strongly increases and additional lines of missing dimer rows are formed perpendicular to the dimer vacancy lines. This is shown in detail in Fig. 5(b), where the missing dimer rows are marked by dotted lines in the high-resolution STM insert. The formation of missing dimer rows is caused by the repulsion between vacancy lines and surface steps.[44] As a result, the (001) terraces completely break up and the (2×8) reconstruction is replaced by a disordered $(m\times n)$ reconstruction, where m and n is at around 10 and 8, respectively.[45,46] More importantly, on the side walls of the grooves a distinct ripple structure appears that is oriented perpendicularly to the stripe direction. This is shown in detail by the STM image of Fig. 5(c) and is also manifested by the appearance of weak {105} spots in the surface orientation map displayed in Fig. 5(a). This transformation becomes even more pronounced when the Ge coverage further increases to 4.3 ML, as demonstrated by the STM images depicted in the lower panel of Fig. 5. At this coverage, the amplitude of the faceted ripple structure has strongly increased and according to the higher-resolution STM images of Figs. 5(e) and 5(f), the ripples consist of alternating {105} microfacets perpendicular to the stripes. Remarkably, these ripples are almost periodic and extend all the way from the top to the bottom of the grooves [cf. Fig. 5(f)]. As shown by the surface profiles across the side wall ripples displayed in Fig. 6(a), the ripples have an average amplitude of ~1 nm and a periodicity of 12–18 nm. This corresponds to an inclination angle of ~8° for the {105} microfacets with respect to the original {11 10} side wall surface, which fits exactly to the surface geometry of the ripples that is illustrated schematically in Fig. 6(b). Since the ripple amplitude is about two times the deposited Ge thickness, a large amount of the Ge deposited into the grooves is contained within the ripple structure, i.e., the ripple intersection must reach down almost to the Si interface.

Ripple formation is driven by two factors: first, for compressively strained Ge, the {105} facets allow a significant lowering of the free surface energy as shown by *ab initio* calculations.[47–49] Second, the three-dimensional (3D) corrugation of the layer also allows a substantial *elastic* strain relaxation due to expansion of the lattice normal to the ripple facets. According to finite element calculations, for a one-dimensional {105} faceted ripple structure about 10% of the strain energy is elastically relaxed.[50] Another important fac-

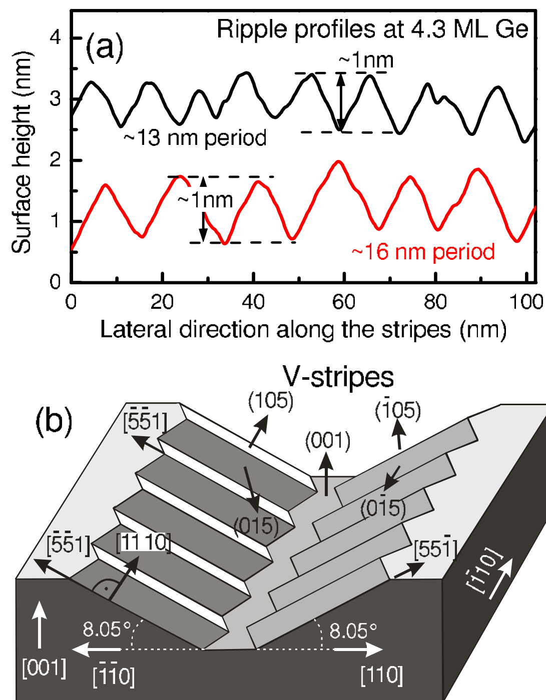

FIG. 6. (Color online) (a) Surface profiles of across the side wall ripples of the "V"-shaped stripe with {11 10} side walls of Fig. 5(f) after 4.3 ML Ge deposition. As indicated by the arrows, the ripple amplitude is around 1 nm and the period in the range of 12–18 nm. (b) Schematic illustration of the {105} microfaceted geometry of side wall ripples. As indicated, the $[\bar{5}\bar{5}1]$ intersection lines between adjacent {105} microfacets are inclined by the 8.05° with respect to the (001) surface. This is exactly equal the inclination angle of the original {11 10} side walls surfaces formed after Si buffer growth. Under this condition, the microfacets can extend without interruption from the top to the bottom of the grooves.

tor for ripple formation is that for the {11 10} "V" grooves, the 8.05° side wall inclination angle equals exactly the inclination angle of the $[\bar{5}\bar{5}1]$ intersection lines of adjacent {105} facets with respect to the (001) surface, as is indicated by the arrow in Fig. 6(b). Under this condition, the {105} ripples can extend without interruption from the bottom to the top of the grooves as observed in Fig. 5(f), facilitating Ge surface diffusion perpendicular to the stripe direction. For grooves with other side wall inclinations or multifaceted "U" geometry, this condition is not fulfilled and therefore such ripples can be formed only in certain parts of the side wall surfaces. This will be shown in detail in Sec. V.

Increasing the Ge coverage further to 4.6 ML, the {105} side wall ripples somewhat coarsen and 3D Ge island nucleation sets in. This is shown by the STM images depicted in Figs. 7(a) and 7(b), where one can see a thickening of the ripples at the "V"-groove bottom. Due to the coarsening process, the intensity of the {105} facet spots in the surface orientation map [insert in Fig. 7(a)] also increases. The few Ge islands nucleate exclusively at the bottom of the grooves and display the typical {105} faceted pyramid structure that is clearly resolved by the high-resolution STM image of Fig. 7(b). As indicated by the insert, nucleation of Ge pyramids proceeds via the formation of shallow mounds as precursors,[51–54] which transform into pyramids once a certain size is exceeded. The {105} pyramids observed at this stage have a very small size of around 1.5 to 3 nm in height and 200 to 900 nm^3 in volume, and the very small density of only a few island per μm^2 indicates that the Ge coverage at the bottom of the groove is just at the onset of the Stranski-Krastanow islanding transition. Further increasing the Ge coverage by 0.3 ML results in a strong increase in the island density and size, as illustrated by the STM images of Figs. 7(c) and 7(d) recorded at 4.9 ML. Evidently, all islands nucleate exclusively at the bottom of the grooves, indicating an efficient downward mass transport along the {105} ripple facets of the side wall surfaces. At this stage the island density increases by a factor of six to $\sim 36\ \mu m^{-2}$ [cf. Fig. 7(d)] and the island height to up to 5 nm, corresponding to a volume increase by more than a factor of 4, but the {105} faceted pyramidal structure is retained. Further increasing the Ge coverage to 5.2 ML as shown in Figs. 7(e) and 7(d) leads to transformation of part of the Ge pyramids to multifaceted domes with additional steeper {113} and {15 3 23} facets[55–57] as indicated in Fig. 7(f). This gives rise to the appearance of the corresponding facet spots in the surface orientation map depicted in Fig. 7(e) as insert. At this stage, also several transitional intermediate island shapes are observed [see Fig. 7(d)]. The island density saturates at around 40 μm^{-2} but the volume of the dome islands is strongly increased to more than 10.000 nm^3 due to the twofold increase in the aspect ratio as well as the increase in the island height to 12–16 nm. At this coverage, the number of still coexisting pyramidal islands is roughly equal to that of the dome islands but at higher coverages (not shown) all pyramids eventually are converted to domes. This is due to the much more efficient elastic energy relaxation of the domes compared to the pyramids (see, e.g., Ref. 56), thus lowering the total energy of the system.

Nucleation of Ge dots at particular surface sites is generally driven by variations in the chemical potential due to variations in either strain or local surface curvature across the substrate surface.[58] The latter is always present on a patterned substrate due to the strong corrugation of the surface topography. The resulting capillary forces generate an enhanced downward adatom flux toward areas with concave surface curvature[1,59] to reduce the overall free surface energy of the sample. This generally leads to a planarization of patterned surfaces during epitaxial growth as already observed during Si buffer growth. For the case of "V"-shaped stripes, the only concave area is at the bottom of the grooves. Therefore, during Ge deposition, material is accumulated at the bottom of the grooves where preferential Ge island nucleation sets in once the local critical wetting layer thickness for the 2D/3D growth transition is exceeded. This is promoted by the much faster surface diffusion of Ge as compared to Si adatoms[60] and as a result, the onset of 3D islanding within the "V" grooves is shifted by 0.5 ML to a smaller critical wetting layer thickness as compared to the growth on planar Si (001). In addition, recent theoretical calculations[61–64] have shown that nucleation of Ge islands in pits or grooves of patterned Si surfaces is also driven by enhanced elastic strain relaxation of islands positioned at concave surface locations, where a significant part of the mismatch strain is accommo-

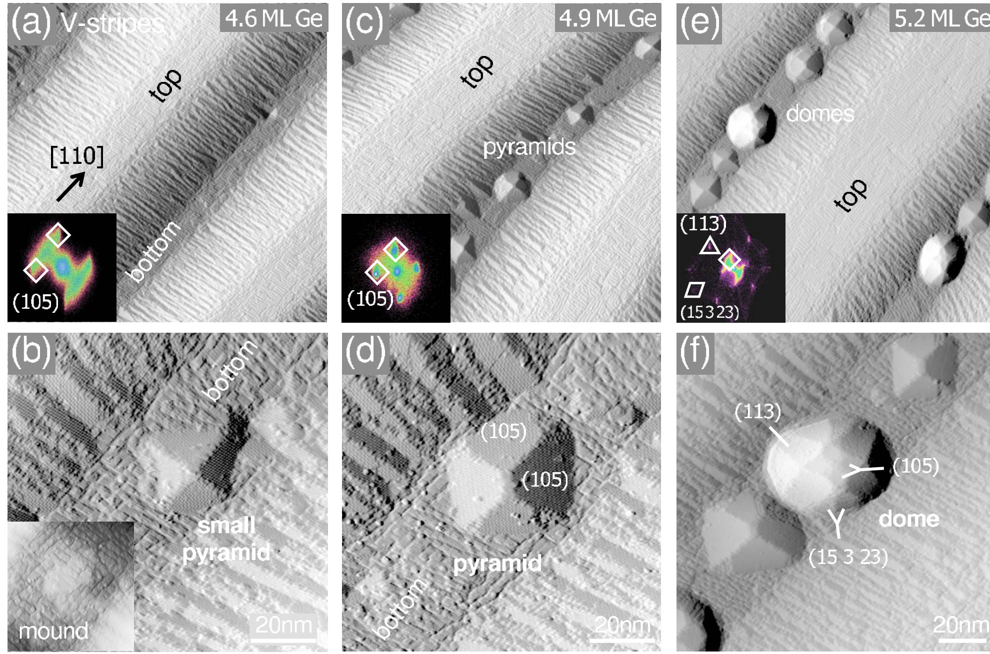

FIG. 7. (Color online) STM images of Ge island nucleation on "V" stripes with {11 10} side walls after 4.6 ML (a,b), 4.9 ML (c,d), and 5.2 ML (e,f) Ge deposition at 600 °C. Overview images (0.5×0.5 μm^2) of the stripes are displayed in the upper panel, details of Ge island structure and their transformation from mounds to pyramids and domes are shown in the lower panel on a magnified scale. The transformation of the island shapes is also manifested by the appearance of additional facet spots in the surface orientation maps shown as inserts.

dated by the substrate lattice,[62,63] which was recently verified by x-ray scattering experiments.[64] Thus, Ge island nucleation at the bottom of the grooves is favored not only by kinetics but also by energetics. That we do not observe Ge island nucleation at other surface sites implies an effective downward mass transport into the grooves. This seems to be provided by the formation of the smooth {105} facets of the side wall ripples because up to the point when ripples are formed no marked difference in the surface structure on the ridges and at the bottom of the grooves is observed, which implies that up to this point there is not much variation in the wetting layer thickness.

V. GE GROWTH ON "U"-SHAPED STRIPES

As shown in Sec. III, at the beginning of the second Si buffer growth, the stripes assume a multifaceted "U" shape with side walls composed of different {11n} facets, starting with shallow {119} areas at the top and bottom of the grooves and steeper {115}, {114}, or {113} facets in the side wall middle. To clarify the role of the Si stripe geometry on Ge growth, in the following, the results for two cases are presented, namely, (a) Ge growth on shallow "U" stripes with only a narrow {115} middle segment, which is obtained just before completion of the transition from "U" to "V"-shaped stripes, and (b) for the case of "U" stripes with steeper and wider {114} side wall segment. As shown below, this small difference in stripe morphology results in a completely different Ge growth and islanding process that changes not only the island sites but also their size and shape as a function of Ge thickness.

A. Growth on shallow "U" stripes with {115} facets

For Ge growth on shallow "U" stripes, STM images recorded after different Ge thicknesses are shown Fig. 8. In this case, the "U" stripes obtained after 10 nm of second Si buffer growth consist of wide, 9° inclined {119} faces at the top and bottom of the groove and a narrow {115} facet near the middle of the side walls. Accordingly, the groove depth is reduced to 30 nm from the initial 40 nm value. During the first Ge deposition step at 520 °C, the stripe morphology is essentially unchanged, i.e., a conformal 2D Ge growth occurs. This is corroborated by the STM images of Fig. 8(a) obtained after 2 ML Ge deposition, where the individual {119} and {115} side wall segments are clearly resolved and exclusively the corresponding facet spots appear in the surface orientation map depicted as insert. As indicated by the high-resolution STM image of Fig. 8(b), at this coverage on top of the ridges the characteristic dimer vacancy lines of the Ge (2×8) surface reconstruction appear, whereas on the {119} side wall areas a D_B double-stepped vicinal surface with ~2 nm terrace width is formed. This is corresponds exactly to the structure observed at 2 ML coverage on "V"-shaped stripes shown in Fig. 4(c). On the contrary, the steeper {115} side wall areas are rather flat, indicating that a stable Ge facet is formed, which agrees with the results of Van Nostrad *et al.*[65] for Ge growth on highly miscut Ge substrates. As shown by Fig. 8(b), on these facet areas, a 2D layer-by-layer Ge growth occurs, which results in the formation of elongated 2D monolayer islands on this side wall region as indicated by the arrow.

When the Ge coverage is increased above 4 ML at 600 °C, {105} ripples appear on the {119} side wall faces near the top and bottom of the grooves, as shown by the

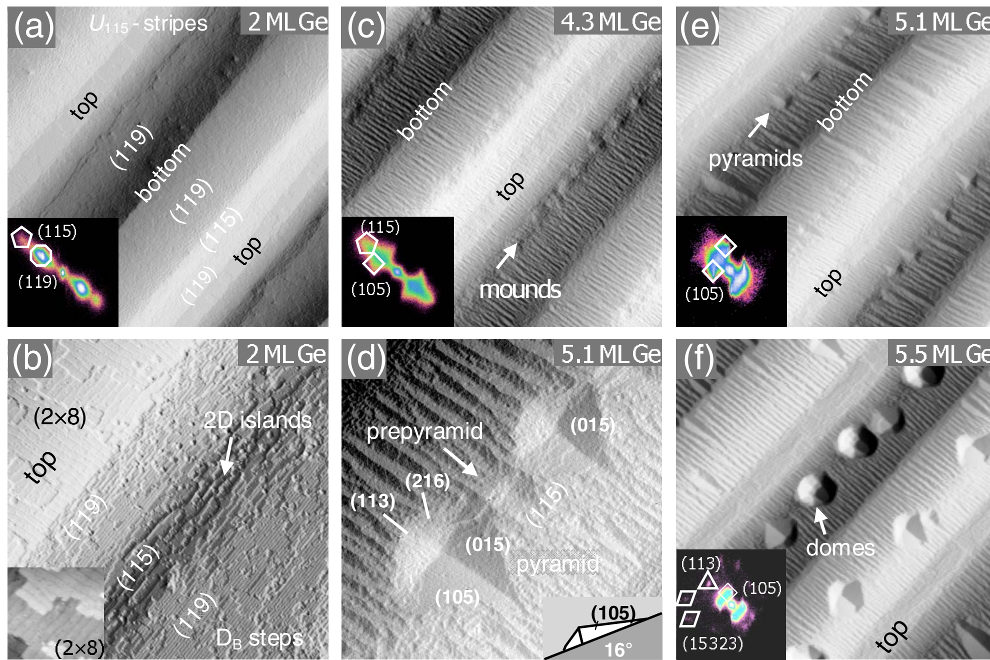

FIG. 8. (Color online) Surface evolution and Ge island growth for shallow "U" stripes with {119} and {115} side wall segments. The Ge thicknesses increases from 2ML at 520 °C to 4.3, 5.1, and 5.5 ML at 600 °C from (a) to (f), respectively. Surface orientation maps are presented as inserts. At 2 ML coverage [(a) and (b)] the sidewall surfaces are still smooth, but 2D islands are formed on the {115} side wall surfaces as indicated by the arrow. At 4.3 ML coverage (c), pronounced side wall ripples are formed on the shallow {119} areas, whereas on the {115} faces mounds are formed as precursors for 3D islands. Increasing the coverage to 5.1 ML [(d) and (e)], the mounds are transformed to small asymmetric pyramids, which subsequently transform into domes at higher coverage (f), while the side wall ripples remain nearly unchanged. Image sizes: 0.5×0.5 μm^2 except in (b) and (d) of 0.2×0.2 μm^2.

STM image displayed in Fig. 8(c) for 4.3 ML coverage. Accordingly, also {105} facet spots appear in the surface orientation map (see insert). The ripples are obviously disrupted by the {115} areal segment along the side wall middle. On these areas, shallow Ge mounds appear that are well visible in the STM image of Fig. 8(c). These mounds have a height of less than 1 nm and represent precursors for subsequent 3D island nucleation. In contrast to the case of "V"-shaped stripes, all mounds are located on the {115} side wall middle and not at the bottom of the grooves. At this coverage, on the top of the flat surface ridges the (2×8) Ge reconstruction is replaced by a $(m\times n)$ reconstruction due to formation of regularly spaced missing dimer rows.

Increasing the coverage to above 5 ML results in transformation of the mounds into asymmetric pyramids as shown in Figs. 8(d) and 8(e) for 5.1 ML coverage. As a result, practically all pyramids are now positioned in the side wall middle of the grooves. The structure of these pyramids significantly differs from the fourfold symmetric {105} pyramids with equal sides formed at the bottom of the "V" grooves or on planar (001) surfaces. As shown by Fig. 8(d), the asymmetric pyramids are terminated at the upper side by two adjacent {105} facets, whereas on the lower edge, the side faces are rather rough and exhibit surface inclinations near {113} and {216}. Although the latter have been reported to be stable Ge facets,[66] according to our STM images they are not well developed on the Ge island side faces. Moreover, since the asymmetric pyramids are sitting on a {115} side wall facet inclined by 16° with respect to the original (001) surface, these pyramids are actually downward looking as is illustrated schematically by the insert of Fig. 8(e). Thus, they have a completely different geometry as compared to usual Ge pyramids. Their growth is mainly fed by step-flow growth from the upper {119} side wall areas, which is evidenced by the downward steps on the upper {105} pyramid facets visible in the STM image displayed in Fig. 8(d). The volume of the pyramids at this coverage ranges from 200 to 2000 nm^3, their height from 1.5 to 3 nm, and their density is about 60 μm^{-2}. With further increasing coverage, the pyramids rapidly grow in size up to $\sim$6000 nm^3 and by 5.5 ML coverage half of them have transformed into large multifaceted dome islands with additionally steeper {113} and {15 3 23} facets. This is illustrated by the STM image displayed in Fig. 8(f), as well as by the corresponding surface orientation map depicted as insert. The domes have a height above 12 nm and volumes exceeding 20.000 nm^3. Because now two rows of dots are formed for each stripe, the island density is a factor of two larger as compared to those on "V" stripes. In contrast to the domes on planar (001) surfaces, the domes also have an asymmetric shape because they are located on the inclined {115} side walls of the grooves. As a result, the upper (113) dome facet is much smaller than the corresponding $(\bar{1}\bar{1}3)$ facet on the lower side of the domes, and the same applies also for the other island facets. Never the less, all facets of the domes are from the same class of facets as for those on planar substrates, i.e., no additional new facet orientations appear.

As shown by Fig. 8(f), for the shallow "U" stripes, nearly all pyramids and dome islands are positioned on the inclined

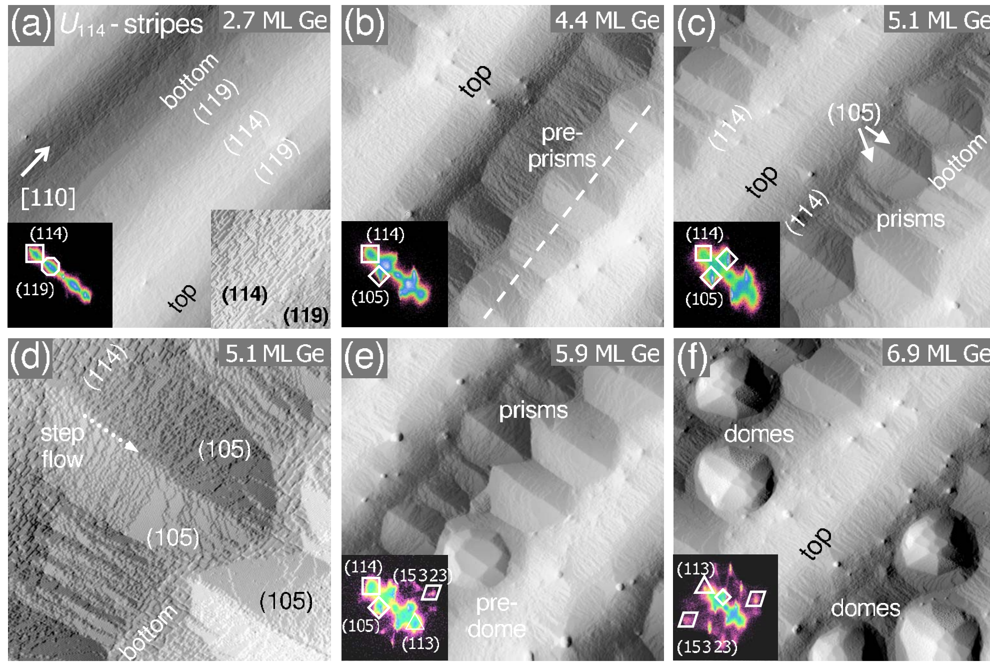

FIG. 9. (Color online) Surface evolution and Ge island growth on steeper "U" stripes defined by {114} and {119} side wall segments. The Ge coverage increases from 2.7, to 4.3, 5.1, 5.9 to 6.9 ML from (a) to (f), respectively, at 600 °C. At 2.7 ML coverage, the side wall surfaces are still smooth, whereas beyond 4 ML coverage ripples are formed on the {119} side wall faces. At 4.4 ML (b), these ripples drastically coarsen such that large {105} faceted prisms are formed on the lower part of the side walls as shown in (c) and (d) for 5.1 ML coverage. At 5.9 ML coverage (e), predome islands start to nucleate on top of the prisms, which transform to the usual Ge domes at coverages beyond 6.5 ML (f). This transition is shown in more detail in Fig. 11. Note that the small spots seen in the STM images are due to growth defects due to long sample storage in UHV. Surface orientation maps are shown as insert and the STM image size is 0.4×0.4 μm^2, except for (d) with 0.2×0.2 μm^2.

{115} side walls of the grooves. According to theoretical calculations,[61–63] from an energetic point of view the most favorable island nucleation sites are surface areas with the largest concave surface curvature at the bottom of the grooves where the largest amount of elastic strain relaxation occurs,[62,63] and this is also what we observe for the case of "V"-groove stripes [see Fig. 7(e)]. However, nucleation of at the bottom of the grooves also requires efficient downward mass transport, which in the case of "U"-shaped stripes is obviously hindered by the steeper {115} segment in the side wall middle of the stripes where consequently, 2D island nucleation and mound formation as precursors for 3D islanding takes place. This indicates that the complex surface kinetics on the nonplanar substrates play an important role for the islanding process. In addition, one has to note that at the intersection of the {115} and lower {119} side wall segments also a concave side wall area is formed, which also promotes local island formation according to the island energetics.[62,63] While the corresponding local curvature is smaller than that at the bottom of the grooves, both kinetic and energetic factors together obviously contribute to the observed Ge islanding at the side wall middle. It is noted, however, that in large-scale STM images of the "U" stripes occasionally also 3D islands are found at the bottom of the grooves, indicating that a competition between side wall nucleation and nucleation at the bottom of the grooves exists.

B. Growth on steeper "U" stripes with {114} facets

For stripes with deeper "U" grooves and steeper {114} side wall segments, the results for Ge growth is displayed in Fig. 9 for coverages from 2.7 to 6.9 ML from (a) to (f), respectively. During the first stage of Ge growth, the stripe geometry is essentially preserved by formation of a conformal wetting layer. As shown by the STM image of Fig. 9(a), at 2.7 ML Ge coverage the side wall geometry is defined by a wider and steeper {114} segment in the side wall middle, followed by shorter {119} segments toward the top and bottom of the grooves. Thus, the overall groove depth is still close to the original 35 nm value and the morphology similar to that observed in Fig. 2(b) after buffer growth. The {119} side wall areas exhibit the usual D_B double-stepped terrace structure as already observed for the other stripe geometries. In contrast to the flat, singular {115} side wall facets of the shallow "U" stripes, however, the {114} side facets consist of a regular downward step train of single monolayer steps and narrow {115} terraces, as is revealed by the high-resolution STM insert of Fig. 9(a). Therefore, on these areas step-flow instead of layer-by-layer growth occurs, i.e., no mounds are formed as precursor islands, in contrast to the case of shallow "U" stripes (Fig. 8). {115} microfacets on miscut Ge substrates have been observed by Van Nostrad et al.,[65] whereas according to Gai et al.,[66] neither {114} nor {115} are stable Ge surfaces because they decompose into {113} and

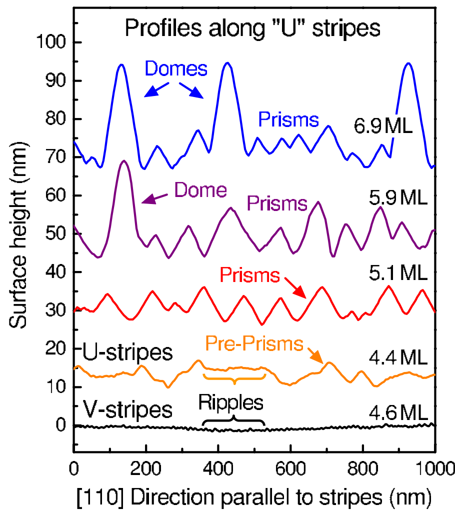

FIG. 10. (Color online) STM profiles along "U"-shaped stripes with {114} side wall faces at Ge different coverages of 4.4, 5.1, 5.9, and 6.9 ML from bottom to top, respectively. The surface profiles were measured along the lower {119} side walls of the stripes as indicated by the dashed line in Fig. 9(b). The surface profile over the side wall ripples of the "V" shaped stripes of Fig. 5(d) at 4.6 ML Ge coverage is shown for comparison as lowest curve on equal scale.

{117} microfacets during high-temperature annealing.

Increasing the Ge coverage to 4.4 ML results in ripple formation on the {119} side wall segments as shown in Fig. 9(b). On the lower {119} side wall faces near the bottom of the grooves, these ripples drastically coarsened to form large-scale undulations along the stripe direction. Remarkably, at even higher Ge coverage of 5.1 ML [see Fig. 9(c)], nearly all ripples on the lower {119} side faces have transformed into huge {105} faceted prisms perpendicular to the stripes. The height of these prisms is as large as 9 nm and their width of up to 120 nm in the stripe direction as demonstrated by the surface profiles displayed in Fig. 10. As shown by the higher-resolution STM image of Fig. 9(d), prism growth is fed by downward step flow from the upper {114} side wall facets onto the prism roofs, whereas the step structure of the adjacent {114} side wall faces remains nearly unchanged. Even at this coverage of 5.1 ML, no Ge pyramids are formed anywhere on the surface [see Fig. 9(c)]. Moreover, the prism volumes exceed those of the usual symmetric {105} pyramids on the "V" stripes by as much as one order of magnitude. This indicates that prism formation represents an effective alternative pathway for strain relaxation and lowering the total energy of the system. This is corroborated by the fact that the prisms display a very rapid growth once the Ge coverage exceeds 4 ML, beyond which their height increases by a factor of ten as compared to amplitude of the initial side wall ripples. Remarkably, these remains unchanged on the upper {119} faces near the edges of the grooves [see Figs. 9(a) and 9(b)]. The growth instability of prism formation is proven by comparison of the surface profiles along side wall surfaces displayed in Fig. 10 as a function of Ge coverage. Whereas the initial side wall ripples observed on the "V" and shallow "U" stripes cease to grow beyond 4 ML Ge coverage and saturate at a ripple amplitude less or equal than 1 nm and periods of 10 to 18 nm (cf. Figs. 5–8), for the "U" stripes with {114} facets at 5.1 ML Ge the prism height and width is as large as 10 and 100 nm, respectively. This difference is illustrated by the profiles of the ripple structure observed for the "V"-shaped stripes of Fig. 6(a) that is depicted in Fig. 10 on the same scale.

When the Ge coverage further increases to 5.9 ML [see Fig. 9(e)], Ge dome island nucleation sets in on top of the prism roofs, which is illustrated in more detail by the STM images presented in Fig. 11. The domes start by building additional {105} and {15 3 23} facets [see Fig. 11(e)], but initially show a considerable variance in size and shapes, indicating that the transformation process from prisms to domes is not completed. At higher Ge coverage of 6.9 ML, most of these transitional domes have assumed an equilibrium shape that closely resembles that of Ge domes islands formed on the other stripe patterns with all characteristic {105}, {113}, and {15 3 23} side facets. This is proven by the STM images of Figs. 9(f) and 11(f) as well as the corresponding surface orientation map depicted as inserts. However, the onset of dome island formation is significantly delayed by as much as 1 ML compared to the case of "V" and shallow "U" stripes, indicating that the large Ge prisms represent an energetically favorable intermediate state that poses a high-activation energy barrier for transformation into the final dome state. This is corroborated by the fact that all domes observed for the steep "U" stripes have rather large sizes with typical ~25 nm height (see Fig. 10) and volumes exceeding 90.000 nm^3, which is a factor of four larger as compared to the domes on the "V" and shallow "U"-shaped stripes.

The overall sequence of transitions of the Ge surface during growth on the steep "U" stripes from smooth side wall facets, to ripples, preprisms, prisms, and prisms with mounds nucleated on the top, to predomes and finally to fully developed domes with increasing Ge coverage is illustrated in detail by the STM images depicted in Fig. 11. Evidently, coarsening and prism growth is fed by downward Ge adatom mass transport from the upper {119} and {114} side wall faces, as is indicated by the dashed arrow in Fig. 11(c). At a critical prism size, 2D islands and mounds nucleate on top of the roof as indicated by the arrow in Fig. 11(d). The measurements yield a critical prism volume of ~50.000 nm^3 or critical height of 11 nm at the onset of this shape transition. With further Ge deposition, the mounds on top of the roofs emerge first into pyramids with four {105} main top facets [see Fig. 11(e)], until stable domes islands are reached [see Fig. 11(f)]. As the domes are located on the inclined side wall part of the grooves, they exhibit a similar asymmetry as the dome islands formed on the side walls of the shallower "U" stripes with {115} facets described in the previous section. In any case, it clearly follows that the islanding process on the steep "U" stripes drastically differs compared to that of the other stripe geometries, demonstrating that the surface topography strongly alters the energetics and kinetics of the process.

The marked difference in island formation as a function of surface geometry is further corroborated by comparing the existence range of the different island shapes as a function of

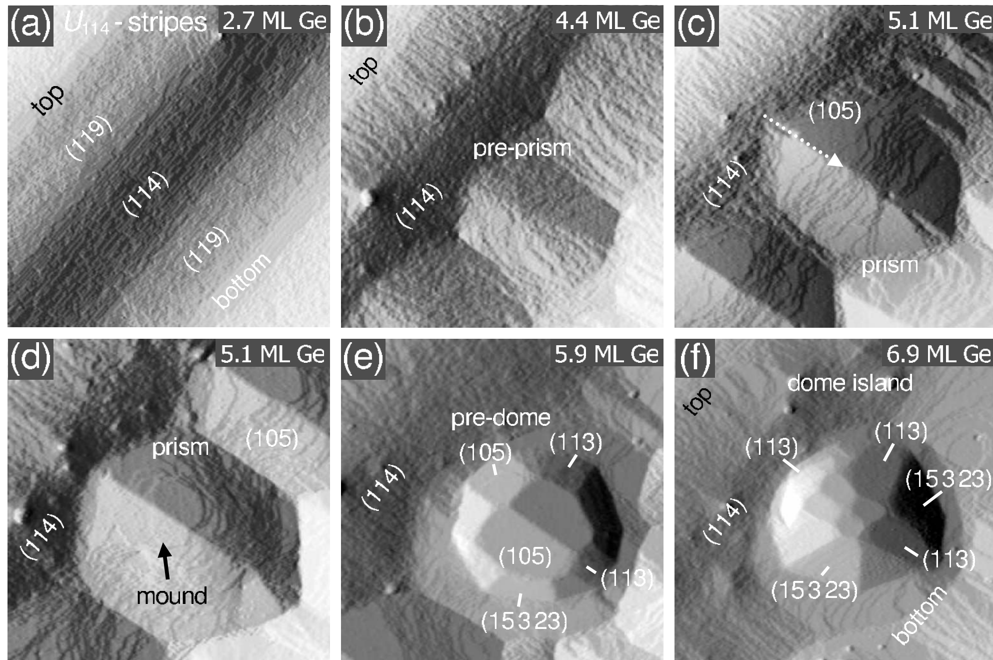

FIG. 11. Details of the Ge island formation process on "U" stripes with {114} side facets for Ge coverages increasing from 2.7, to 4.4, 5.1, 5.9, and 6.9 ML from (a) to (f), respectively (image size 0.2×0.2 μm^2). At 3 ML coverage (a), the side wall surfaces are still very smooth, whereas beyond 4 ML coverage, ripples are formed on the upper and lower {119} side wall faces. With increasing Ge coverage, the ripples drastically coarsen (b) until large {105} faceted prisms (c) are formed on the lower side wall areas, which are fed by step-flow Ge growth from the upper {119} side faces at the top of the grooves as indicated by the dashed arrow. Beyond 5.7 ML, nucleation of additional Ge 2D islands at the roof of the prisms sets in (d), which leads to the nucleation of predomes and domes on top of the prisms as shown in (e) and (f), respectively. While the topography on the {119} are drastically changes with increasing Ge coverage, the {114} steeper sidewall segments remain nearly unchanged.

size for different stripe geometries as well as for Ge growth on unpatterned Si (001) performed under the same conditions. The results are summarized in Fig. 12 in the form of bar graphs for all four cases of Ge growth on (i) a flat 2D Si (001) surface, as well as on stripe-patterned substrate templates with (ii) "V," (iii) shallow "U_{115}," and (iv) steeper "U_{114}" side walls from top to bottom, respectively. For the planar 2D surface and "V"-shaped stripes, nearly the same transitions from mounds to symmetric {105} pyramids and finally multifaceted domes occurs, where the latter is separated by a transitional region marked by TD in Fig. 12, in which the islands exhibit various intermediate shapes between ideal pyramids and domes. The critical island size at which these transitions occur are quite similar for the two cases, i.e., pyramids are formed at a critical island size of about 200 nm^3 and the transformation of pyramids into domes starts at a critical pyramid size of $\sim$4.000 nm^3 or critical height of 5 nm. This similarity is due to the fact that in both cases 3D island formation essentially takes place on a planar (001) surface region (bottom of the grooves for the "V" stripes). Thus, also the identical island shapes are produced. Due to downward mass transport, however, the onsets of pyramid, respectively, dome formation occurs about 0.5 ML earlier for the "V"-shape stripes compared to the planar surface, which is the mechanism for positioning of the Ge islands along the bottom of the grooves.

For the shallow "U" stripes with {115} facets, asymmetric pyramids are formed on the side walls instead of square {105} pyramids [see Fig. 8(d)] at a critical size of about 400 nm^3 and these "V" pyramids obviously persist to a larger critical size of up to 8.000 nm^3 before they start to transform into dome islands. For the steeper "U" stripes with {114} facets, elongated prisms are formed instead of pyramidal islands. This proceeds by a rather continuous coarsening of the initial side wall ripple structure at Ge thicknesses ex-

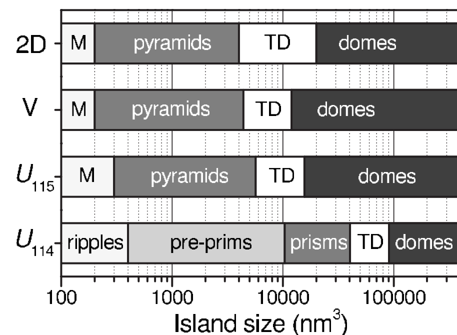

FIG. 12. Schematic illustration of the size ranges for mounds (m), pyramids, transitional domes (TD) and domes for Ge growth on either a 2D (001) Si surface, "V"-shaped stripes with {11 10} sides faces, shallow "U" stripes with {115} facets and steeper "U" stripes with {114} facets from top to bottom, respectively. For the latter, the surface evolves from ripples, preprisms, prisms, and transitional domes to completed domes with increasing size and increasing Ge coverage. Ge growth was performed under the same conditions for all cases at a substrate temperature of 600 °C.

ceeding 4 ML. As a result, a very wide transitional region of preprisms with various sizes and intermediate shapes [see Fig. 9(b)] exists such that there is no obvious critical thickness or critical size for prism formation. On the other hand, the onset of precursor domes on top of the prisms does not begin before the prisms have reached a critical size of 40.000 nm^3, which much exceeds the size of the domes on the planer surface or "V" stripes. Correspondingly, the smallest dome size observed on steep "U" stripes is a factor of four larger as in the other three cases. Remarkably, the onset of dome formation on top of the prisms sets in at a Ge thickness about one monolayer *larger* as compared to the flat 2D Si surface, whereas for the other stripe geometries the islanding onset is at smaller critical coverages. These findings demonstrate that islanding process is drastically altered by the surface topography.

Finally, it is also instructive to compare the mean island-island distances for the four different growth cases. Along the stripe direction, the mean island distance is calculated from the average dot density along the stripe direction. For the three types of stripe geometries, more or less the same average dot distance of about 120 nm is obtained. For the unpatterned 2D reference sample, the average dot distance is taken as the inverse square root of the areal 2D dot density, which yields a value of 240 nm at the same growth conditions. This factor of two difference indicates that Ge mass transport parallel to the stripes is strongly reduced on the patterned surfaces. This is caused by the side wall ripple formation, which allows an effective mass transport perpendicular to the stripes along the ripple facets but not across the ripples along the stripe direction. The latter reduces the adatom capture zones of the islands in the stripe direction, resulting in nucleation of islands much closer to each other as compared to a planar surface. This factor should be taken into account for optimization of the growth process.

VI. CONCLUSIONS

In conclusion, the systematic investigation of Si and Ge growth onto stripe-patterned Si substrates has unraveled a characteristic and well-defined surface evolution that sensitively depends on stripe geometry as well as deposited layer thicknesses. The differences in stripe geometry strongly affect the self-assembly process of Ge nanoislands and, as a result, Ge islands may nucleate either in the middle or on the side walls of the grooves. The stripe geometry can be controlled by Si buffer growth, during which the initial surface topography evolves from multifaceted "U" shapes to a final "V" shape by successive transformations from steeper {113} side wall facets over {114} and {115}, and finally to {11 10} facets. Ge growth on these stripes first induces a substantial surface roughening before the actual onset of island formation, which is characterized by the appearance of {105} side wall ripples oriented perpendicular to the stripe direction. For "V"-shaped stripes, these ripples extend all the way from the top to the bottom of the grooves where Ge island nucleation occurs due to efficient downward mass transport. On the contrary, for multifaceted "U" stripes, the side wall ripples are interrupted in the middle by steeper side wall segments. This strongly modifies the nucleation process such that mounds and subsequently, pyramids and domes align on the side walls rather than the bottom of the grooves. The island shapes also depend on their position on the stripe topography and ranges from square pyramids, to asymmetric pyramids or elongated prisms, but all eventually converge into dome islands at higher Ge coverages. The island position also affects the critical coverages for island nucleation that is reduced for "V" stripes but increased for "U" stripes. A similar effect is also found for the critical island sizes for the shape transitions. The striking differences reveal that kinetics as well as energetics play important roles for the self-assembly process on prepatterned substrate templates. Thus, precise control of the pattern morphology is essential for site-control and practical device applications.

ACKNOWLEDGMENTS

We thank Alma Halilovic for technical assistance and Friedrich Schäffler and Moritz Brehm for discussion. This work was supported by the Austrian Science Funds (Grants No. SFB-IRON and No. P17436-N08) and by the Gesellschaft für Mikro- und Nanoelektronik.

*bolormaa.sanduijav@jku.at
†Corresponding author. gunther.springholz@jku.at

[1] A. Hartmann, L. Vescan, C. Dieker, and H. Lüth, J. Appl. Phys. **77**, 1959 (1995); L. Vescan, K. Grimm, M. Goryll, and B. Holländer, Mater. Sci. Eng., B **69–70**, 324 (2000).
[2] T. I. Kamins and R. Stanley Williams, Appl. Phys. Lett. **71**, 1201 (1997).
[3] A. Konkar, A. Madhukar, and P. Chen, Appl. Phys. Lett. **72**, 220 (1998).
[4] O. G. Schmidt, N. Y. J. Phillipp, C. Lange, U. Denker, K. Eberl, R. Schreiner, H. Gräbel-dinger, and H. Schweizer, Appl. Phys. Lett. **77**, 4139 (2000).
[5] D. S. L. Mui, D. Leonard, L. A. Coldren, and P. M. Petroff, Appl. Phys. Lett. **66**, 1620 (1995); H. Lee, J. A. Johnson, J. S. Speck, and P. M. Petroff, J. Vac. Sci. Technol. B **18**, 2193 (2000).
[6] O. G. Schmidt, S. Kiravittaya, Y. Nakamura, H. Heidemeyer, R. Songmuang, C. Müller, N. Y. Jin-Phililpp, K. Eberl, H. Wawra, S. Christiansen, H. Gräbeldinger, and H. Schweizer, Surf. Sci. **514**, 10 (2002).
[7] Z. Zhong, A. Halilovic, T. Fromherz, F. Schäffler, and G. Bauer, Appl. Phys. Lett. **82**, 4779 (2003).
[8] D. Grützmacher, T. Fromherz, C. Dais, J. Stangl, E. Mueller, Y. Ekinci, H. H. Solak, H. Sigg, R. T. Lechner, E. Wintersberger, S. Birner, V. Holy, and G. Bauer, Nano Lett. **7**, 3150 (2007).
[9] Z. Zhong, O. G. Schmidt, and G. Bauer, Appl. Phys. Lett. **87**, 133111 (2005).
[10] B. Yang, F. Liu, and M. G. Lagally, Phys. Rev. Lett. **92**, 025502 (2004).

[11] G. Chen, H. Lichtenberger, G. Bauer, W. Jantsch, and F. Schäffler, Phys. Rev. B **74**, 035302 (2006).
[12] Z. Zhong, A. Halilovic, M. Mühlberger, F. Schäffler, and G. Bauer, Appl. Phys. Lett. **82**, 445 (2003); J Appl. Phys. **93**, 6258 (2003).
[13] C. Dais, H. H. Solak, Z. Ekinci, and D. Gruetzmacher, Surf. Sci. **601**, 2787 (2007).
[14] Gang Chen, Vastola, H. Lichtenberger, D. Pachinger, G. Bauer, W. Jantsch, F. Schäffler, and Leo Miglio, Appl. Phys. Lett. **92**, 113106 (2008).
[15] B. Sanduijav, D. Matei, G. Chen, F. Schäffler, G. Bauer, and G. Springholz, Thin Solid Films **517**, 293 (2008).
[16] I. Berbezier and A. Ronda, Phys. Rev. B **75**, 195407 (2007); Surf. Sci. Rep. **64**, 47 (2009).
[17] A. Karmous, I. Berbezier, A. Ronda, R. Hull, and J. Graham, Surf. Sci. **601**, 2769 (2007).
[18] S. Kiravittaya, A. Rastelli, and O. G. Schmidt, Appl. Phys. Lett. **87**, 243112 (2005); Rep. Prog. Phys. **72**, 046502 (2009).
[19] C. Teichert, Phys. Rep. **365**, 335 (2002).
[20] B. Sanduijav, D. Matei, G. Chen, and G. Springholz, Mater. Sci. Semicond. Process. (to be published).
[21] *Handbook of Silicon Wafer Cleaning Technology*, edited by K. R. Reinhardt and W. Kern (William Andrew, Norwich, 2007).
[22] H. Lichtenberger, M. Mühlberger, and F. Schäffler, Appl. Phys. Lett. **82**, 3650 (2003).
[23] M. Grundner and H. Jacob, Appl. Phys. A **39**, 73 (1986).
[24] S. R. Kasi, M. Liehr, P. A. Thiry, H. Dallaporta, and M. Offenberg, Appl. Phys. Lett. **59**, 108 (1991).
[25] A. A. Baski, S. C. Erwin, and L. J. Whitman, Surf. Sci. **392**, 69 (1997).
[26] D. J. Chadi, Phys. Rev. Lett. **59**, 1691 (1987).
[27] S. Song and S. G. J. Mochrie, Phys. Rev. B **51**, 10068 (1995).
[28] T. Suzuki, H. Minoda, Y. Tanishiro, K. Yagi, H. Kitada, and N. Shimizu, Surf. Sci. **357-358**, 73 (1996).
[29] J. Knall, J. B. Pethica, J. D. Todd, and J. H. Wilson, Phys. Rev. Lett. **66**, 1733 (1991).
[30] J. Dabrowski, H. J. Müssig, and G. Wolff, Phys. Rev. Lett. **73**, 1660 (1994).
[31] D. M. Bird, L. J. Clarke, R. D. King-Smith, M. C. Payne, I. Stich, and A. P. Sutton, Phys. Rev. Lett. **69**, 3785 (1992).
[32] M. Hanbücken, B. Röttger, and H. Neddermeyer, Surf. Sci. **331–333**, 1028 (1995).
[33] B. S. Swartzentruber, N. Kitamura, M. G. Lagally, and M. B. Webb, Phys. Rev. B **47**, 13432 (1993).
[34] J. de Miguel, C. E. Aumann, R. Kariotis, and M. G. Lagally, Phys. Rev. Lett. **67**, 2830 (1991).
[35] J. E. Griffith, G. P. Kochanski, J. A. Kubby, and P. E. Wierenga, J. Vac. Sci. Technol. A **7**, 1914 (1989).
[36] U. Köhler, O. Jusko, B. Müller, M. Horn-von-Hoegen, and M. Pook, Ultramicroscopy **42-44**, 832 (1992).
[37] F. Wu and M. G. Lagally, Phys. Rev. Lett. **75**, 2534 (1995).
[38] B. Voigtländer and M. Kästner, Phys. Rev. B **60**, R5121 (1999).
[39] B. Voigtländer, Surf. Sci. Rep. **43**, 127 (2001).
[40] R. Butz and S. Kampers, Appl. Phys. Lett. **61**, 1307 (1992).
[41] J. Tersoff, Phys. Rev. B **45**, 8833 (1992).
[42] F. Liu and M. G. Lagally, Phys. Rev. Lett. **76**, 3156 (1996).
[43] P. D. Szkutnik, A. Sgarlata, A. Balzarotti, N. Motta, A. Ronda, and I. Berbezier, Phys. Rev. B **75**, 033305 (2007).
[44] P. Sutter, I. Schick, W. Ernst, and E. Sutter, Phys. Rev. Lett. **91**, 176102 (2003).
[45] I. Goldfarb, J. H. G. Owen, P. T. Hayden, D. R. Bowler, K. Miki, and G. A. D. Briggs, Surf. Sci. **394**, 105 (1997).
[46] A. Rastelli, H. von Känel, G. Albini, P. Raiteri, D. B. Migas, and L. Miglio, Phys. Rev. Lett. **90**, 216104 (2003).
[47] G. H. Lu, M. Cuma, and F. Liu, Phys. Rev. B **72**, 125415 (2005); G. H. Lu and F. Liu, Phys. Rev. Lett. **94**, 176103 (2005).
[48] V. B. Shenoy, C. V. Ciobanu, and L. B. Freund, Appl. Phys. Lett. **81**, 364 (2002).
[49] C. O. E. Shklyaev, M. J. Beck, M. Asta, M. J. Miksis, and P. W. Voorhees, Phys. Rev. Lett. **94**, 176102 (2005).
[50] G. Vastola (private communication).
[51] P. Sutter and M. G. Lagally, Phys. Rev. Lett. **84**, 4637 (2000).
[52] R. M. Tromp, F. M. Ross, and M. C. Reuter, Phys. Rev. Lett. **84**, 4641 (2000).
[53] J. Tersoff, B. J. Spencer, A. Rastelli, and H. von Känel, Phys. Rev. Lett. **89**, 196104 (2002).
[54] A. Rastelli, H. Von Känel, B. J. Spencer, and J. Tersoff, Phys. Rev. B **68**, 115301 (2003).
[55] G. Medeiros-Ribeiro, A. M. Bratkovski, T. I. Kamins, D. A. A. Ohlberg, and R. S. Williams, Science **279**, 353 (1998).
[56] F. M. Ross, J. Tersoff, and R. M. Tromp, Phys. Rev. Lett. **80**, 984 (1998).
[57] F. M. Ross, R. M. Tromp, and M. C. Reuter, Science **286**, 1931 (1999).
[58] G. Springholz, in *Handbook of Self-assembled Semiconductor Nanostructures for Novel Devices in Photonics and Electronics*, edited by M. Henini (Elsevier, Oxford, 2008), p. 1 (and references therein).
[59] G. Biasiol, A. Gustafsson, K. Leifer, and E. Kapon, Phys. Rev. B **65**, 205306 (2002).
[60] Li Huang, F. Liu, G.-H. Lu, and X. G. Gong, Phys. Rev. Lett. **96**, 016103 (2006).
[61] R. V. Kukta and D. Kouris, J. Appl. Phys. **97**, 033527 (2005).
[62] H. Hu, H. J. Gao, and F. Liu, Phys. Rev. Lett. **101**, 216102 (2008); H. Wang, Y. Zhang, and F. Liu, J. Appl. Phys. **104**, 054301 (2008).
[63] Zhenyang Zhong, W. Schwinger, F. Schäffler, G. Bauer, G. Vastola, F. Montalenti, and L. Miglio, Phys. Rev. Lett. **98**, 176102 (2007).
[64] T. U. Schülli, G. Vastola, M.-I. Richard, A. Malachias, G. Renaud, F. Uhlík, F. Montalenti, G. Chen, L. Miglio, F. Schäffler, and G. Bauer, Phys. Rev. Lett. **102**, 025502 (2009).
[65] J. E. Van Nostrand, S. Jay Chey, and D. G. Cahill, Phys. Rev. B **57**, 12536 (1998).
[66] Zheng Gai, R. G. Zhao, Xiaowei Li, and W. S. Yang, Phys. Rev. B **58**, 4572 (1998).